Space Webs

Final Report

Authors: David McKenzie, Matthew Cartmell, Gianmarco Radice, Massimiliano Vasile
Affiliation: University of Glasgow

ESA Research Fellow/Technical Officer: Dario Izzo

Contacts:

Matthew Cartmell
Tel: +44(0)141 330 4337
Fax: +44(0)141 330 4343
e-mail: m.cartmell@mech.gla.ac.uk

Dario Izzo
Tel: +31(0)71 565 3511
Fax: +31(0)71 565 8018
e-mail: act@esa.int

Available on the ACT website
http://www.esa.int/act

Ariadna ID: 05/4109
Study Duration: 4 months
Contract Number: 4919/05/NL/HE

Contents

Abstract

The use of large structures in space is an essential milestone in the path of many projects, from solar power collectors to space stations. In space, as on Earth, such large projects may be split into more manageable sections, dividing the task into multiple replicable parts. Specially constructed spider robots could assemble these structures piece by piece over a membrane or space-web, giving a methodology for building a structure while on orbit.

The stability of the space web will be critical to many applications, such as solar power generation, and this will be affected by the movement of the spider robots. In an attempt to mitigate this, the dynamics of the space-web with movement of the robots are investigated. Simulations of the space-web plus robot system will show that space-webs can take a variety of different forms, and this report gives some guidelines for configuring the space-web system either to minimise the movement of the web with a given mass of robot or to estimate the maximum web dimensions or mass given a robot specification.

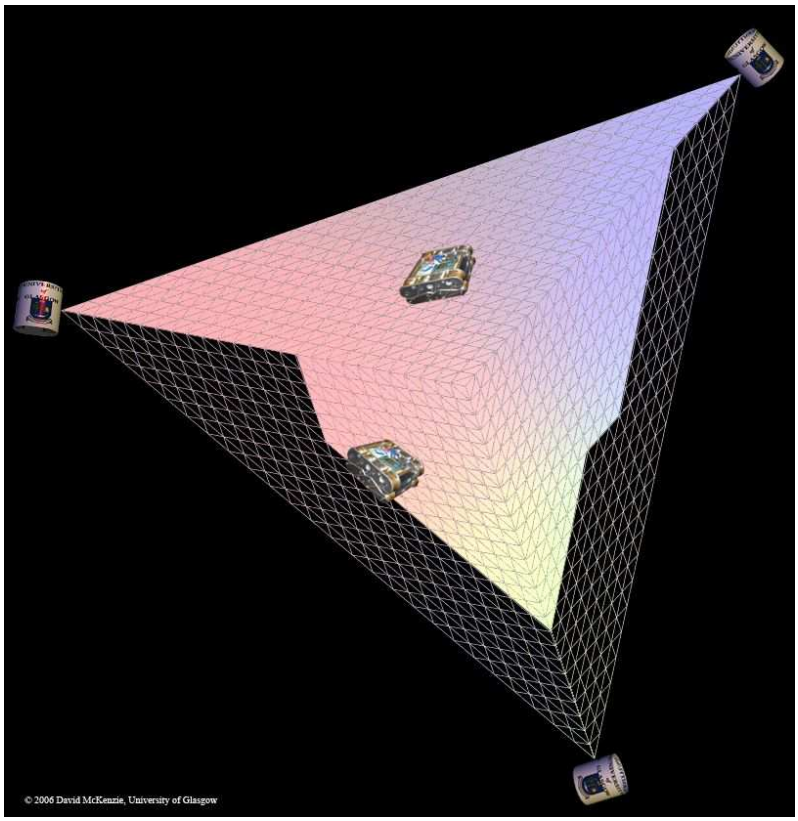

Chapter 1

Introduction

For years humanity has dreamed of a clean, inexhaustible energy source. This dream has lead many people to do what, in retrospect, seems obvious, and look upward toward nature's 'fusion reactor', the sun. However, while sunlight is clean and inexhaustible[1], it is also dilute and intermittent. These problems led Peter Glaser to suggest in 1968 that solar collectors be placed in geostationary orbit [Glaser, 1968]. Such collectors are known as solar power satellites (SPS). A solar power satellite is a proposed satellite operating in high Earth orbit that uses microwave power transmission to beam solar power to a very large antenna on Earth where it can be used in place of conventional power sources. The advantage to placing the solar collectors in space is the unobstructed view of the Sun, unaffected by the day/night cycle, weather, or seasons.

The SPS essentially consists of three parts: a huge solar collector, typically made up of solar cells; a microwave antenna on the satellite, aimed at Earth; a rectifying antenna, or rectenna, occupying a large area on Earth to collect the power. For best efficiency the satellite antenna must be between 1 and 1.5 kilometres in diameter and the ground rectenna around 14 kilometres by 10 kilometres. For the desired microwave intensity this allows transfer of between 5 and 10 GW of power. To be cost effective it needs to operate at maximum capacity. To collect and convert that much power the satellite needs between 50 and 150 square kilometres of collector area thus leading to huge satellite design. Huge is by no means an understatement. Most designs are based on a rectangular grid some 10 km per side, much larger than most man-made structures here on Earth. While certainly not beyond current engineering capabilities, building structures of this size in orbit has

[1] for a few billion years anyway!

never been attempted before.

Without a doubt, the biggest problem for the SPS concept is the currently immense cost of all space launches. Gerard O'Neill noted this problem in the early 1970s, and came up with the idea of building the SPSs in orbit with materials from the Moon. More recently the SPS concept has been suggested as an application for the space elevator. The elevator would make construction of SPSs considerably less expensive, possibly making them competitive with conventional sources. However it appears unlikely that even recent advances in materials science, namely carbon nanotubes, could reduce the price of construction of the elevator enough in the short term.

One possible alternative approach to the on-orbit assembly of such a massive structure would be the use of webs [Kaya et al., 2004a] [Kaya et al., 2004b]. A large net-like structure could firstly be deployed in orbit. Once the net is stabilised, spiderbots could be used to crawl over the net towards specified locations and move solar cells into the desired positions. Essentially the net or thin membrane provides a deployable fundamental infrastructure on which the spiderbots could be used to construct the specific superstructure required for the completion of the SPS.

This has two advantages:

1. a generic web infrastructure may be used, and
2. various SPS morphologies could be constructed, modified, and deconstructed, as required.

This study will consider the fundamental conceptual design of an appropriate and generic thin membrane, its orbital mechanics, and therefore its deployment and on orbit maintenance.

A model of a net in orbit is presented here, with robots moving along the surface of the net, simulating reconfiguration of the system. Useful guidelines to the initial conditions of the net and components are found and give a starting point for further studies into the field.

Studies have previously shown that robots may be deployed in this way to reconfigure the net structure [Kaya et al., 2004a], [Nakano et al., 2005], and plans are underway to test the concept on a sounding rocket.

This new class of structures with robots moving over the surface will be defined as 'Space-Webs', with the robots correspondingly named 'Spiderbots'.

In summary the objectives of the study are:

- To accurately model the space-web system
- To understand the post-deployment and stabilisation dynamics of the space-web in an orbital environment
- To investigate the factors influencing the stability of the space-web
- Finally, validation of the models developed through appropriate test-case scenarios

Chapter 2

Literature Review

Tethers have had a long and interesting history, beginning when the father of astronautics, Konstantin Tsiolkovsky, looked up at the newly constructed Eiffel Tower in Paris in 1895 and conceived the Space Elevator.

The history of tether missions is given in a particularly accessible book by Bekey [Bekey, 1983], as well as a good overview of tether dynamics and the concept of using constellations in tether missions. Tether technology has progressed in these two decades to include the dynamics of tethers on orbits [Beletsky et al., 1993] and the extension of the material technology to counteract the hostile environment of space [Forward and Hoyt, 1995]. An extensive tether guide may also be found in the 'Tethers in Space Handbook' [Cosmo and Lorenzini, 1997], covering the fundamental dynamics of tethers, the challenges of operating a tether in orbit and giving details about tether missions, including the TSS-1R satellite flown on the Space Shuttle.

Not limited to dumbbell tethers, the Motorised Momentum Exchange Tether (MMET) was conceived to propel payloads further and faster [Cartmell, 1998], with Cartmell [Cartmell et al., 2004] and Ziegler [Ziegler and Cartmell, 2001] investigating the dynamics of this new configuration and validating the equations with a ground test [Cartmell and Ziegler, 2001]. New avenues of research have been opened by Draper, investigating the feasibility of the MMET system [Draper, 2006], McKenzie, researching length deployment of the tether and using a novel trajectory for the MMET [McKenzie and Cartmell, 2004], and Murray, using the MMET to continuously transfer payloads to the Moon [Murray et al., 2006].

Using tethers as a structure on which to lay the membranous structures is not a new idea. Solar sail configurations have been using methods similar to these extensively, for example [McInnes, 1999] [Masumoto et al., 2006]. Tethers

were also simultaneously considered as an alternative to stationkeeping for controlling satellites while flying in formation [Cosmo et al., 2005].

The two concepts of tethers and membranes or webs rarely overlap, with the Japanese researchers Kaya [Kaya et al., 2004a] and Nakano [Nakano et al., 2005] pioneering the idea of using the traditional Furoshiki (folding cloth) with reconfigurable robots reconfiguring the web surface. Equilibrium conditions for tethered three-body systems are described by Misra [Misra, 2002], but are not immediately applicable to the web system.

One of the few papers [Palmerini et al., 2006] investigating the dynamics of space-webs found that the orbiting 2D web was not a stable configuration and recommended that rotation of the web is necessary to achieve stability.

One thing is clear, the dynamics of the space-web system would undoubtedly be complex, and has warranted further attention [Fujii et al., 2006].

Chapter 3

Modelling of Space-webs

3.1 Introduction

Space-webs have one definite advantage over single use spacecraft: the ability to reconfigure the web to suit the mission or environment. Due diligence must therefore be observed to ensure that the act of reconfiguring the web does not endanger the web or satellite. Investigating the movement of the robots while moving over the web is essential: the movement of their mass and momentum may significantly affect the web dynamics.

The stability of the system is to be investigated while the robots crawl along the web surface in two pre-defined motions:

- Three robots simultaneously moving along the outer catenaries of the web
- Three robots simultaneously moving from the centre to the outside of the web

3.2 Modelling Methodology

This study will aim to develop an analytical model of the space-web system that can be numerically integrated on a desktop PC in a time of the order of minutes. This is in contrast to the ESA ACT study undertaken by KTH [Tibert and Gärdsback, 2006] which models the system with much higher fidelity, but takes in the order of days to numerically integrate.

When constructing a numerical simulation of an existent system, it is important to consider that the simulation can only be said to represent a real life scenario when the model has been validated and the initial conditions used in the calculation are representative of the simulation scenario.

This may seem like an obvious statement, but these facts are often overlooked for convenience or speed.

In modelling the space-web, it is important to make the modelling process transparent and verifiable. In this spirit, the steps followed to assemble the space-web model are outlined paying particular attention to the steps followed to produce a model in *Mathematica* and the process of validating the model against previous models and the real life case where possible.

3.3 Web Meshing

3.3.1 Web Structure

To gain an accurate estimate of the energy of the web, the mass distribution over the web is discretized [Ziegler, 2003]. An algorithm has been designed in *Mathematica* to take the triangle bounded by the i^{th} sub-span, the $(i+1)^{th}$ sub-span and the facility mass and divide this into equally sized smaller triangles.

The space-web is modelled as s sub-spans, clustered around the central facility mass. Each sub-span is considered to be rigid and massless, held rigid by the centripetal force of rotation around the centre of mass. An idealized point mass m_i is placed at the end of the sub-span, at length l_i, with the position of each endpoint mass given by $P_{i_{local}}$ in Equations 3.5, 3.6.

The web is stretched between the sub-spans i and $i+1$ and replicated to give s triangular webs. Each triangular web section is idealised as an elastic plane containing the mass of that section, however the internal elastic forces within the web are not modelled at this stage.

3.3.2 Dividing the Web

Each web section is divided into n equal sections (referred to here as 'divisions'), in the direction given by the line joining the midpoint of the sub-span ends and the facility, as represented in Figures 3.1 to 3.3.

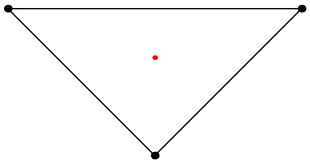

Figure 3.1: 0 divisions

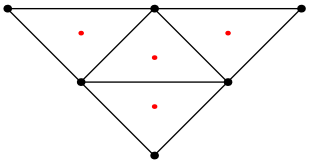

Figure 3.2: 1 division

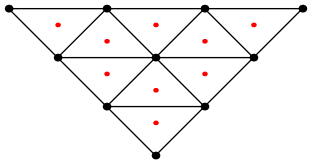

Figure 3.3: 2 divisions

For each of the n web sections;

triangles	=	$(n+1)^2$
triangles in top row	=	$2n+1$
row configuration	=	$\{2n+1, 2(n-1)+1,$
		$2(n-2)+1, \ldots, 3, 1\}$
number of rows	=	$n+1$
nodes	=	$\frac{1}{2}(n+2)(n+3)$
midpoints	=	$(n+1)^2$

3.3.3 Web Divisions

A point mass is placed at each mid-point, therefore the total number of masses for the webs are $s(n+1)^2$, where s is the number of sub-spans. That is to say, the number of masses in the web increases as the square of the number of divisions. This can lead to a very large number of mass points to consider for a fine-grain web.

Assembling the space-web with three sub-spans ($n = 3$) and 0 divisions gives the layout shown in Figure 3.4, with Figure 3.5 showing the same layout with 1 division, and finally Figure 3.6 shows the same layout with 2 divisions. Each red dot is a mass-point on the web.

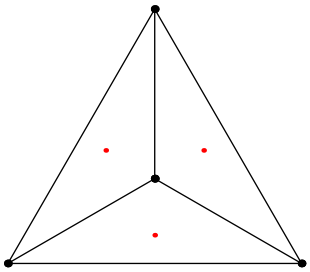

Figure 3.4: 3 sub-spans - 0 divs

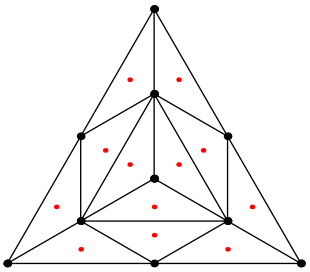

Figure 3.5: 3 sub-spans - 1 div

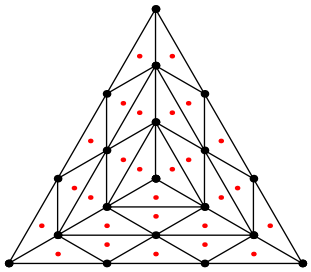

Figure 3.6: 3 sub-spans - 2 divs

The space-web layout may be expanded to analyse different web configura-

tions. A square layout with 1 division per section is shown in Figure 3.7; a pentagonal layout with 2 divisions per section is shown in Figure 3.8; and a hexagonal layout with 3 divisions per section is shown in Figure 3.9 with total of 103 masses[1].

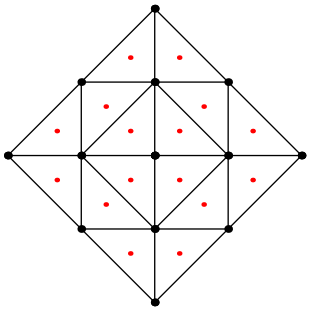

Figure 3.7: 4 sub-spans - 1 div

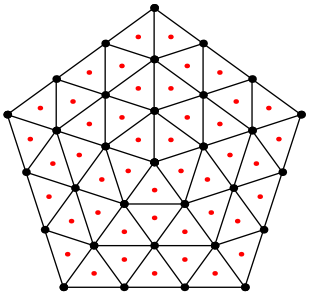

Figure 3.8: 5 sub-spans - 2 divs

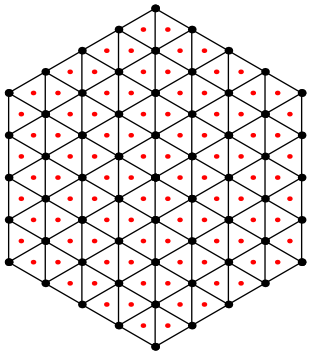

Figure 3.9: 6 sub-spans - 3 divs

3.4 Equations of Motion

3.4.1 Centre of Mass Modelling

In a real world scenario, the mass of the web is likely to be unevenly distributed. Modelling this requires an expression for the centre of mass (CoM) position, in this case using the facility mass as the origin.

For n masses with positions $\{X_i, Y_i, Z_i\}$, the position of the Centre of Mass about the Facility, in terms of the local $\{X, Y, Z\}$ coordinate system centred on the Facility mass, is:

$$P_{Facility \rightarrow CoM} \left\{ \frac{\sum_{i=1}^{n} M_i X_i}{\sum_{i=1}^{n} M_i} , \frac{\sum_{i=1}^{n} M_i Y_i}{\sum_{i=1}^{n} M_i} , \frac{\sum_{i=1}^{n} M_i Z_i}{\sum_{i=1}^{n} M_i} \right\} \tag{3.1}$$

This is used in later equations by taking the position *from* the Centre of Mass *to* the Facility mass, as $P_{CoM \rightarrow Facility} = -P_{Facility \rightarrow CoM}$

[1] 103 masses = 96 web midpoints + 6 sub-span masses + 1 central facility mass

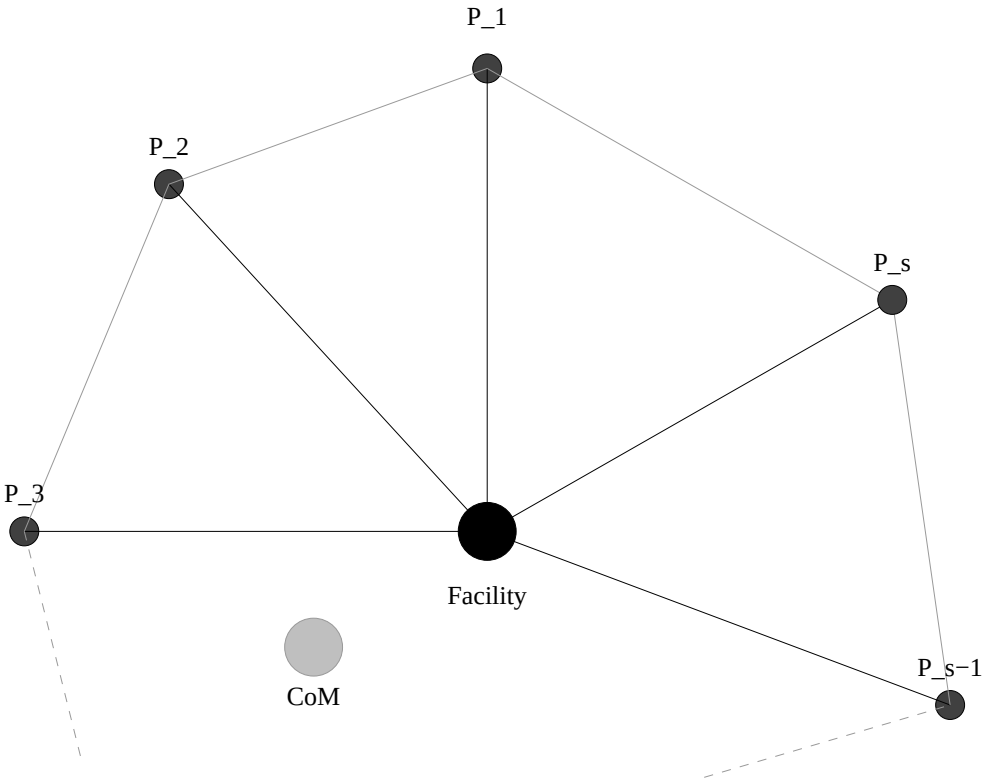

Figure 3.10: Simplified Space-web layout with s sub-spans

3.4.2 Rotations

Rotational matrices are used to rotate the starting vectors to their positions on the local and inertial planes. The local position vector in Equation 3.5 is the matrix product of a series of rotations. A diagram of the space-web configuration is shown in Figure A.1 with the web removed for clarity.

$$R_{\psi_i,X} = \begin{bmatrix} 1 & 0 & 0 \\ 0 & \cos[\psi_i] & -\sin[\psi_i] \\ 0 & \sin[\psi_i] & \cos[\psi_i] \end{bmatrix} \tag{3.2}$$

$$R_{\alpha_i,Y} = \begin{bmatrix} \cos[\alpha_i] & 0 & \sin[\alpha_i] \\ 0 & 1 & 0 \\ -\sin[\alpha_i] & 0 & \cos[\alpha_i] \end{bmatrix} \tag{3.3}$$

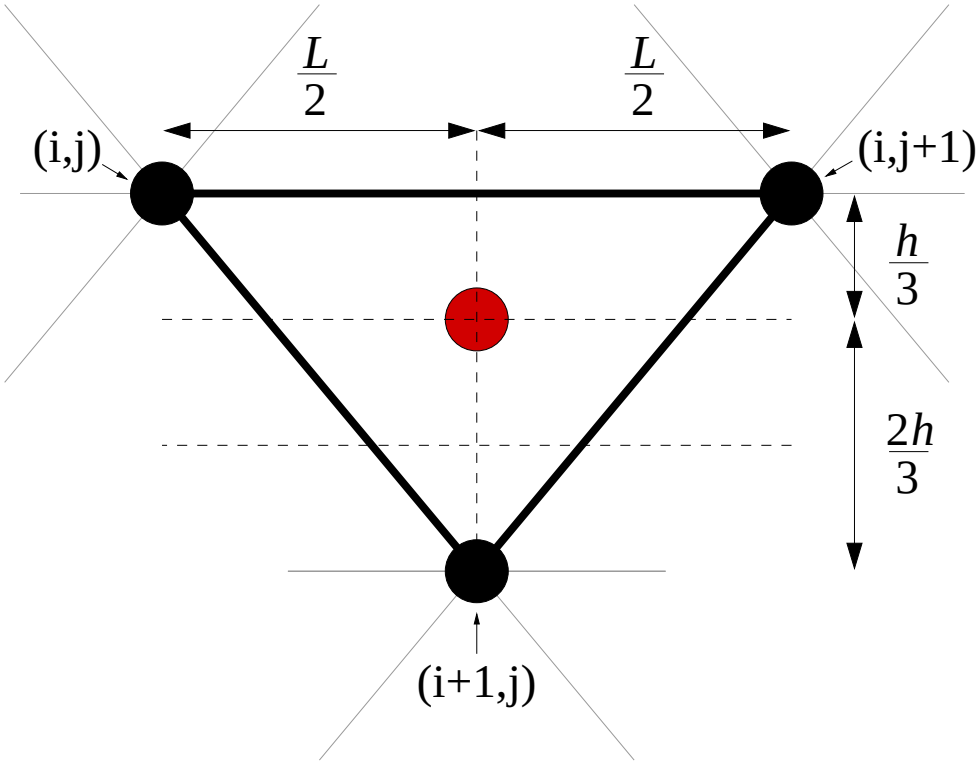

Figure 3.11: Midpoint location

$$R_{\phi_i,Z} = \begin{bmatrix} \cos[\phi_i] & -\sin[\phi_i] & 0 \\ \sin[\phi_i] & \cos[\phi_i] & 0 \\ 0 & 0 & 1 \end{bmatrix} \tag{3.4}$$

$$P_{i_{Local}} = R_{\psi_i,X}.R_{\alpha_i,Y}.R_{\phi_i,Z}.L_i \tag{3.5}$$

where $L_i = \{0, 0, l_i\}^T$, aligned along the local Z axis

$$P_{i_{inertial}} = R_{\theta,Z}\left(P_{0\rightarrow CoM} - P_{Facility\rightarrow CoM} + (R_{\psi_i,X}.R_{\alpha_i,Y}.R_{\phi_i,Z}.L_i)\right) \tag{3.6}$$

Rotations may be performed using the rotation order X then Y then Z:

The sub-span is rotated around the facility by an angle ψ with the axis of rotation in the X-axis only. This vector is then rotated around the facility by an angle α with the axis of rotation in the Y-axis only. Finally, this vector is then rotated around the facility by an angle ϕ with the axis of rotation in the Z-axis only.

The angles are projected about their respective axes i.e., the Z-rotation, ϕ, is contained in the $X-Y$ plane. The angles themselves can be compared to the standard aerospace rotations, with the sub-span direction from the facility to the edge taken as the tail-nose direction. In this case: ψ is the yaw angle, in the plane of the space-web; α is the pitch angle, out of the space-web plane; and ϕ is the roll angle, the twist in the sub-span.

Considering rotations about the ψ direction only - that is constraining the motion of the space-web to be in-plane - gives the following equation

$$P_{i_{inertial}} = R_{\theta,Z}\left(P_{0\rightarrow CoM} - P_{Facility\rightarrow CoM} + (R_{\psi_i,X}.L_i)\right) \tag{3.7}$$

Where $P_{0\rightarrow CoM} = \{R, 0, 0\}$, and represents the position of the Centre of Mass from Earth and $R_{\psi_i,X}$ is the rotation of the sub-span about the central facility given by Equation 3.2.

3.4.3 Position equations

The positions of the masses in the local coordinate system must be translated and rotated into the inertial (Earth centred) coordinate system. The local position vectors are added to the position vector from the CoM to the Facility and the position vector from the Earth to the CoM. The resultant vector is then rotated into the Earth centred Inertial axis system.

3.5 Energy Modelling

For every mass point in the system with position in the inertial frame, P_i, the following steps are undertaken in order to find the Lagrangian energy expression L:

the respective velocities, V_i are found:

$$V_i = \frac{\partial}{\partial t} P_i \tag{3.8}$$

the kinetic energies (linear T_{lin} and rotational T_{rot}) are obtained and summed:

$$T_{lin} = \sum_{i=1}^{n} \frac{1}{2} m_i V_i.V_i \tag{3.9}$$

$$T_{rot} = \sum_{i=1}^{n} m_i \frac{1}{2} P_{i_{local}} . P_{i_{local}} \frac{(\psi_1' + \psi_2' + \psi_3')^2}{3} \tag{3.10}$$

the potential energies, U, are obtained and summed:

$$U = \sum_{i=1}^{n} \frac{\mu m_i}{\sqrt{P_i . P_i}} \tag{3.11}$$

and the Lagrangian is found:

$$L = T_{rot} + T_{lin} - U \tag{3.12}$$

The moment of inertia of each mass point on the web is calculated using the parallel axis theory about the central facility, then multiplied by the square of the average angular velocities of the three sub-spans to give the rotational kinetic energy.

The average angular velocity of the three sub-spans, as shown in Equation 3.13, was chosen in preference to the actual calculated angular velocities of each mass point to simplify the Lagrangian energy expression and to lighten the computational load. Instead of 27 individual angular velocities, every mass point on the web was assumed to have one common angular velocity. There is an error in this assumption, but this will be acceptably small because the actual velocity is approximately equal to the average velocity.

$$\left(\frac{\partial \psi}{\partial t} \right)_{ave} = \frac{1}{3} \left(\frac{\partial \psi_1}{\partial t} + \frac{\partial \psi_2}{\partial t} + \frac{\partial \psi_3}{\partial t} \right) \tag{3.13}$$

For each mass point, the Lagrangian energy expression is constructed by considering the total kinetic and potential energies of the system.

$$\frac{d}{dt} \left(\frac{\partial T}{\partial \dot{q_j}} \right) - \frac{\partial T}{\partial q_j} + \frac{\partial U}{\partial q_j} = Q_j \tag{3.14}$$

Lagrange's Equations are generated for all the generalised coordinates as specified in Equation 3.14.

The elastic force the web imparts on the sub-span ends are modelled as a simple elastic tether [Miyazaki and Iwai, 2004], obeying Hooke's Law;
$F = Kx$:

$$F = K\left(H\left[(P_i - P_{i+1}) - \frac{2\pi}{s}\right]\right) \tag{3.15}$$

where H[...] is the Heaviside function.

The forces are then used to calculate the right hand side of Lagrange's Equations, Q_i, through consideration of the virtual work.

3.5.1 Simplifying Assumptions

To solve the full set of Lagrange's Equations for this space-web system in a reasonable time on a desktop PC requires some simplifying assumptions to be made.

Firstly, five generalised coordinates are chosen defining the space web rotating in the plane normal to the radius vector: $(R, \theta, \psi_1, \psi_2, \psi_3)$. The diagram in Figure A.1 shows the layout of the space-web, where R is the orbital Radius, θ is the true anomaly, ψ_n is the angle between the n^{th} sub-span and the X_{local} coordinate system.

If the out-of-plane motion of the space-web were to be included, this would increase the number of generalised coordinates to eight, as each sub-span must have the out-of-plane motion defined.

If the space-web orbits exclusively in-plane, a simplifying assumption may be performed in terms of the potential energy expression:

$$U = \sum_{i=1}^{n} \frac{\mu m_i}{R} \tag{3.16}$$

3.5.2 Robot Position Modelling

Robots may move across the space-web in order to reconfigure the web or other tasks as discussed previously. To model this as an kinetic energy based term while retaining the flexibility of defining the path without hard-coding this into the equations, the robot position vector needs to be kept in a very general form.

The robot position vector in Equation 3.17 is defined similarly to Equation 3.6: a vector addition of the R vector, the CoM vector and the vector defining the local position of the robot where

$\{PRobot_X, PRobot_Y, PRobot_Z\}_{local}$ are the local vector positions of the robot in the X, Y, Z axes with the origin coincident on the facility mass.

$$PRobot_{inertial} = R_{\theta,Z}(P_{0\rightarrow CoM} - P_{Facility\rightarrow CoM} + \{PRobot_X, PRobot_Y, PRobot_Z\}_{local}) \tag{3.17}$$

The robot local position vector may be a function of time, position of the sub-span masses (ψ_1, ψ_2, ψ_3), an arbitrary path function or any other smooth generalised function.

The kinetic energies of the robot (both linear and rotational) are derived from the positions of the robot as before. Both the Lagrangian energy expression and Lagrange's Equations contain terms for the local position, velocity, and acceleration of the robots.

Keeping the robot position functions in the most general form allows for rapid reconfiguration of the robot paths and may lead to, for example, robot control studies in the future.

Chapter 4

Space-web Dynamics

4.1 Dynamical Simulation

The space-web dynamics are heavily governed by the centre-of-mass movement of the system. The space-web system is very rarely symmetrical (both in reality and in simulations) and this asymmetry can lead to unstable and even chaotic motion in certain configurations of the space-web.

Several different parameters were considered to be possible influences on the stability of the space-web system, including:

- variation of the masses of the web
- the masses of the robots, the sub-span and facility masses
- the position and velocity of the robots
- the general angular momentum of the robots
- the angular velocity of the web
- and the starting configuration of the web or 'web symmetry'

4.2 Investigating the Stability of the Space-web

To test the stability of the space-web with robot movement over the web, two general cases (out of an initial range of six) with different robot movements have been considered.

Firstly, a symmetrical case with three robots moving anticlockwise on the perimeter of the web, is shown in Figure A.20, labelled 'Case 1'. Secondly, a single robot moving from the central facility to the outer edges of the web along the first sub-span, is shown in Figure A.21, labelled 'Case 6'. Both figures may be found in the Appendix.

Clearly, the robot movement will have an impact on the stability, but there are many factors to be considered alongside this. As momentum is a vector quantity, the sum of the robot's momentum is more important than a single robot. For example, it is possible that three symmetrical robots moving with coordinated trajectories may perturb the web less than a single moving robot.

4.2.1 Mass of the web

The mass of the web was found to have a negative impact on the stability of the system. The higher the mass of the web, the more likely the triangle is to deform from the perfect equilateral shape, and the more likely the system is to exhibit chaotic motion. This is likely to have been due to the increase in the ratio of the web mass to the other masses, causing the web mass to dominate the other mass terms. Figures A.2, A.3, A.4, A.5, A.6 and A.7 demonstrate this effect, which were simulated with Case 1* in which only the mass of the web is varied.

Runs 5-8 show the space-web can be stabilised while the robots move across the surface, the mass of the web increasing to a critical value of approximately 25% of the total system mass. The maximum CoM displacement is $0.78m$ for these four runs. In runs 9-10, the mass of the web is increased to $40kg$ and $48kg$ respectively. This causes significant instability in the web for the $48kg$ web, showing that for certain configurations of the space-web system, the mass of the web is a critical parameter.

4.2.2 Robot crawl velocity

The faster the robots travelled along the web, the greater the likelihood of unstable behaviour of the web, as the CoM displacement plots show in Figures A.18 and A.19. Both are simulated with Case 6 - asymmetrical robot paths.

When robot crawl velocity was reduced from $1.0m/s$ to $0.1m/s$, keeping the run time fixed at $1000s$, the maximum CoM displacement was reduced by

*runs 5-11 B, with symmetrical robot paths

more than an order of magnitude - from $30m$ to $1m$.

These two cases of mass dependant stability and velocity dependant stability are clearly energy related. The higher the energy contained in the system, the more likely the system is to exhibit unstable behaviour. This boundary has not yet been clearly defined. Generally speaking, however, the slower the robot movement across the web, the more likely the web is to remain stable.

4.2.3 Robot mass

The momentum of the robot was thought to be a significant parameter in the stability of the space-web, therefore the robot mass was investigated as a possible parameter. Runs 18-21 tested values of Mrobot from $10kg$ to $100kg$* and the CoM positions are shown in Figures A.8, A.9, A.10 and A.11.

Increasing the mass of the robot did not cause any major instabilities in the space-web system for the narrow range of initial conditions tested. This did have the unintended effect of highlighting a resonance between the robot movement and the system. For the $10kg$ and $20kg$ robots, the system CoM location can be seen to orbit with a cam-like locus. The $50kg$ and $100kg$ robots caused the CoM of the system to describe an epitrochoid shape, rather like the rotor of a Wankel engine.

4.2.4 Web Asymmetry

The single biggest driver of instability on the space-web system was found to be the asymmetry in the web configuration and mass distribution.

Very small asymmetries in the initial conditions of the space-web (compared to a perfectly symmetrical equilateral triangle) are amplified in certain configurations of the space-web, and may create large instabilities in the system, especially for energetic configurations such as high web mass and/or large angular velocities. A small difference in orientation (on the order of $1°$) of the sub-spans may lead to large asymmetries between the sub-spans in a relatively short time ($\approx 100s$).

The cases chosen to investigate the effect of asymmetry on the web are as follows:

- Case 1: Robots 1,2,3 walk along the edges of the web from sub-span to next sub-span - (symmetrical)

*from 3.4% to 17.1% of the system mass

- Case 2: Robots 2,3 walk along the edges of the web while Robot 1 is stationary on sub-span 1 - (unsym.)
- Case 3: Robot 3 walks along the edges of the web while Robots 1,2 are stationary on sub-spans 1,2- (unsym.)
- Case 4: Robots 1,2,3 walk along from the centre to their sub-spans - (sym.)
- Case 5: Robot 1 spirals outwards from the centre to the edges, Robots 2,3 are fixed on sub-spans (unsym.)
- Case 6: Robot 1 walks along from the centre to sub-span1, Robots 2,3 remain in centre (unsym.)

Cases 1 and 4 are symmetrical, shown in Figures A.12 and A.12. These have a stable CoM position throughout the simulation, with a maximum CoM travel of only $0.6m$. In contrast, Cases 2, 3, 5 and 6 are asymmetrical, shown in Figures A.13, A.14, A.16, and A.17. The asymmetric cases show a large CoM movement of between $15m$ and $40m$, and are unstable.

Compounding the problem of uneven mass, the initial conditions of the three sub-spans were found to influence the stability of the system. The equations could not be solved with $\psi = \{0°, 120°, 240°\}$ or spacing the web sub-spans by exactly 120°, for reasons not known at this time. Initial conditions for ψ were implemented as a triplet; the three sub-span values of $\{0+\psi, 120°, 240° - \psi\}$ offer a solution to this problem.

More generally, it is expected that for most configurations of the triangular space-web, holding the three sub-spans permanently rigid at exactly 120° separation will be impossible as small perturbations to the web in the space environment will be constantly experienced.

Adding the effect of many asymmetrical robot masses exacerbates the problem of uneven mass distribution. To remedy this, the space-web must be configured to occupy as low an energy state as the mission will allow: low web mass; light, slow moving robots; low angular velocity of the web. In this state, the asymmetry of the web still exists, but it is kept to a manageable level.

4.3 Numerical Investigation into Stability

A series of solutions to the space-web equations of motion were examined to examine the effect of five parameters on the space-web stability. The mass of the web, $Mweb$, the mass of the three daughter satellites, $Msat$, the robot mass, $Mrobot$, the sub-span angular coordinate, ψ and the average sub-span angular velocity $\frac{\partial \psi}{\partial t}$ were thought to have an effect on the maximum movement of the Centre of Mass (CoM) of the space-web system. Therefore, the solutions to 36 different sets of initial conditions were found, with $2^5 = 32$ runs complemented by 4 centre point runs. The 36 runs were performed in Mathematica, and the results of the maximum CoM displacement were entered into a statistical package, Design Expert 7.03. Design Expert then performs an analysis of variance (ANOVA) calculation on the factorial data provided. ANOVA is a collection of statistical models and their associated procedures which compare means by splitting the overall observed variance into different parts. A 5 degree of freedom model (or less, if requested) is then extrapolated from the data and analysed for statistical significance.

The five most strongly correlated model parameters were: $Mweb-$, $Msat+$, $Mweb * \frac{\partial \psi}{\partial t}+$, $Msat * Mrobot * \frac{\partial \psi}{\partial t}-$, $Mrobot-$ and $Mrobot * Msat-$.

$\psi+$ and $\frac{\partial \psi}{\partial t}-$ were statistically relevant in the model, but to a lesser degree than the other parameters. As they have a stronger effect when combined with other variables, the (un)stabilising influence they have may be overtaken by these other factors.

Parameters are shown with a $(+)$ indicating a stabilising effect or a $(-)$ indicating a destabilising effect, with the full table of values located in the Appendix.

As $Mweb-$ has the strongest influence over the model, it would be most beneficial to the stability to reduce the mass of the web.

The reverse is true of the daughter satellite mass, $Msat+$, increasing this parameter will tend to stabilise the system.

For combinations of main parameters such as $Mweb * \frac{\partial \psi}{\partial t}+$, it would be most beneficial to increase the product to stabilise the system. In this case, the angular momentum of the web will tend to rigidize the system and enhance the stability.

4.3.1 Masses of the Web and Satellite

The influence the masses of the web and the daughter satellites have on the CoM position are shown in the contour graph, Figure 4.1. The contours are shaded from blue (stable) through green and yellow to red (unstable) and follow the maximum CoM displacement from the central facility.

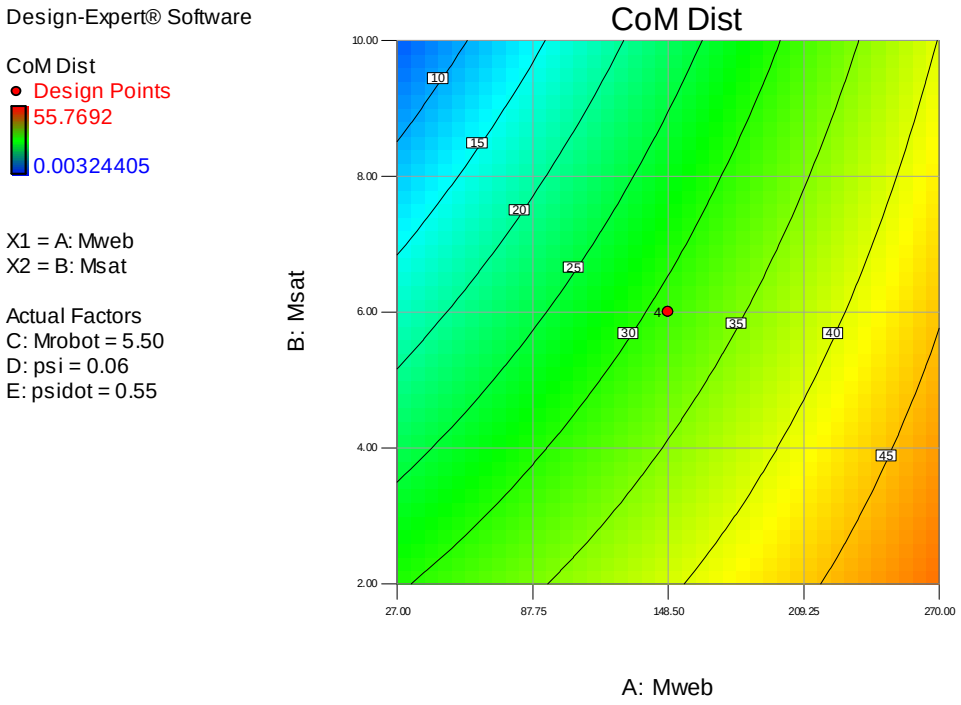

Figure 4.1: CoM movement while varying Web and Satellite Mass

For the small sample space of initial conditions, the most stable point would be a high satellite mass ($> 8kg$) and low web mass ($< 50kg$). A CoM displacement of above $10m$ is unstable, and would be very difficult for a robot to manoeuvre over the surface.

In general terms, this clearly shows the stabilising effect of the mass of the satellites and the destabilising effect of the mass of the web.

4.3.2 Masses of the Web and Robot

The influence the masses of the web and the robot have on the CoM position are shown in the contour graph, Figure 4.2. The contours are shaded from blue (stable) through green and yellow to red (unstable) and follow the maximum CoM displacement from the central facility.

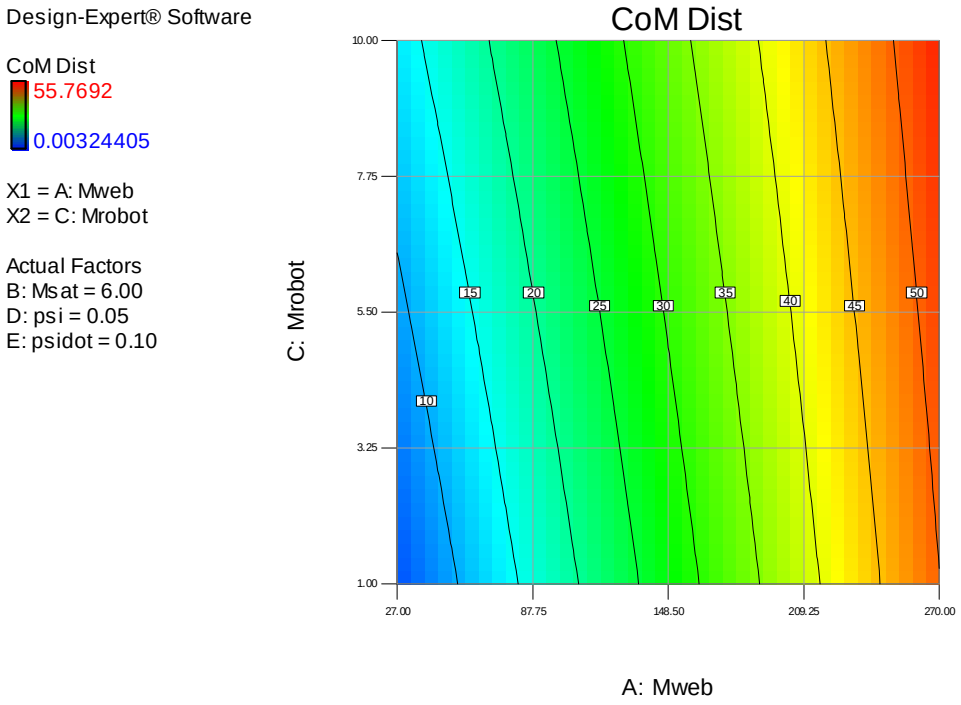

Figure 4.2: CoM movement while varying Web and Robot Mass

The relative strengths of the robot and web masses are shown, with the mass of the web exerting a much stronger influence over the behaviour of the web. The stability boundary is shown in the bottom left hand corner of the graph. A stability margin of $5m$ is preferable, here the web mass must be kept below $50kg$ and the mass of the robot, although less influential, would be best suited at below $5kg$. This shows that if a low $\frac{\partial \psi}{\partial t}$ is required, the web can be made more stable with careful consideration of variables.

4.3.3 Mass of the Web and Angular Velocity

The influence the masses of the web and the angular velocity, $\frac{\partial \psi}{\partial t}$, have on the CoM position are shown in the contour graph, Figure 4.3. The contours are shaded from blue (stable) through green and yellow to red (unstable) and follow the maximum CoM displacement from the central facility.

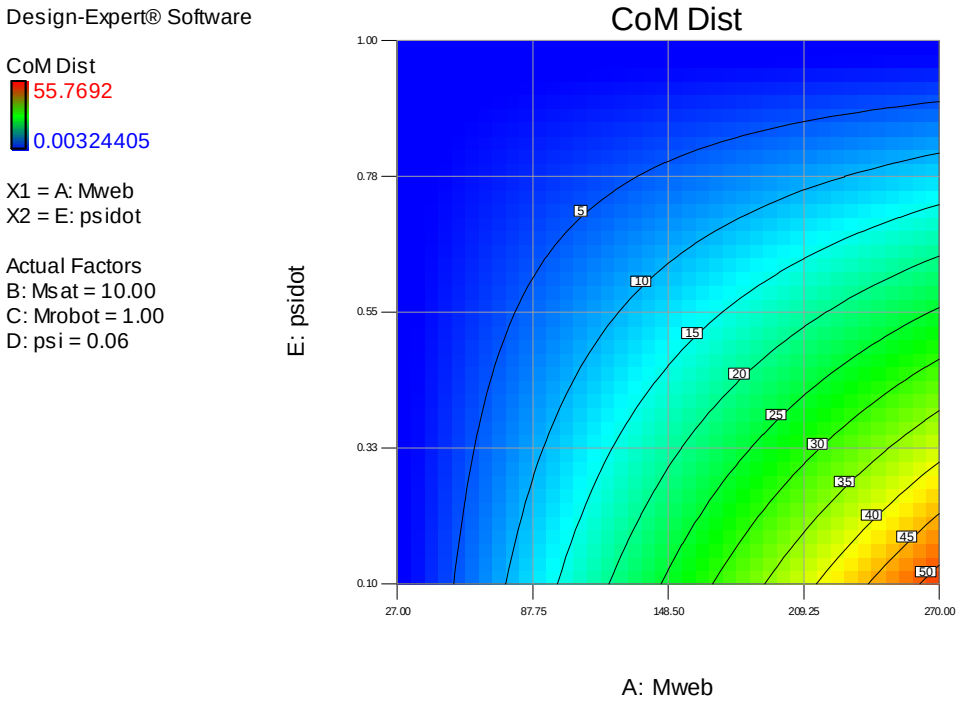

Figure 4.3: CoM movement while varying Web Mass and $\frac{\partial \psi}{\partial t}$

In a high-stability scenario, the options to configure the space-web are plentiful. Carefully choosing the previous parameters that lead to a high probability of stability, namely a high satellite mass ($10kg$) and a low robot mass ($1kg$), affords a larger range of possible values for the mass of the web and the angular velocity of the web.

If the largest acceptable CoM movement is limited to $5m$, then there are three choices available, depending on the primary requirement of the space-web system. If a low web mass is required, then a low $\frac{\partial \psi}{\partial t}$ must match, and vice versa. Alternatively, if a high mass is required, a high $\frac{\partial \psi}{\partial t}$ must be specified, and vice versa. The final option is for a low web mass and a

high $\frac{\partial \psi}{\partial t}$, affording a large safety margin that may be advantageous in, for example, a pilot study mission.

4.3.4 Mass of the Robot and Angular Velocity

The influence the mass of the robot and the angular velocity, $\frac{\partial \psi}{\partial t}$, have on the CoM position are shown in the contour graph, Figure 4.4. The contours are shaded from blue (stable) through green and yellow to red (unstable) and follow the maximum CoM displacement from the central facility.

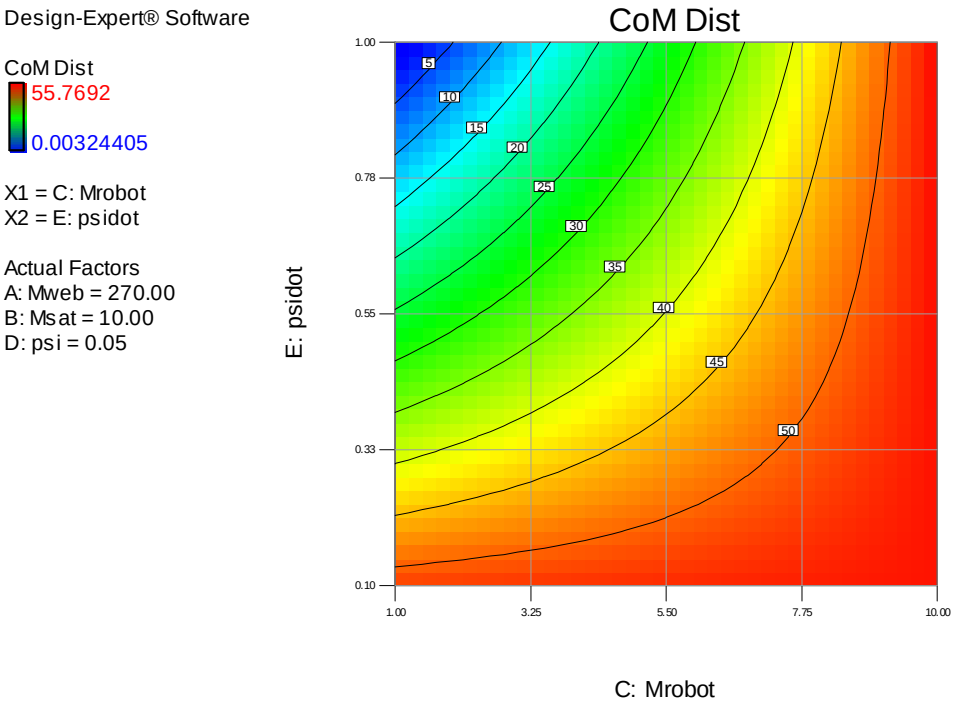

Figure 4.4: CoM movement while varying Robot Mass and $\frac{\partial \psi}{\partial t}$

The final comparison is for a high mass specification - a $270kg$ web mass and $10kg$ satellite mass. This combines the two strongest influences on the system, the former destabilising and the later stabilising. For a stable system, it is essential to ensure the robot mass is small and the angular rotation rate is large.

Chapter 5

Conclusions

5.1 Conclusions

The achievement of a stable, re-configurable web orbiting in space with robots moving along its surface is a realistic goal. There must, however, be limits to the behaviour of the robots and the configuration of the web. Both the robots and the web must be as light as possible and the robots must be as slow moving as the mission allows, given that this limits the destabilising effects of these parameters. The daughter satellites must be as heavy as possible, and the angular rotation rate must be as large as possible to maximise these stabilising effects. In all cases, the web configuration must be as symmetrical as practicable.

5.2 Future Work

To capitalise on the knowledge gained in this research, there are a few areas that may be expanded on for potential future exploration.

Constructing the web while on orbit would mitigate the deployment phase of the mission, eliminating one of the major failure modes of the system. Using the robots to weave the web could be inspired by spiders on Earth, for example, just as the space web has been inspired by the Furoshiki cloth.

Using the knowledge gained through moving masses over the web, there are many applications that would benefit from simulating web-based constructions with moving masses. Solar-sails and antennae could be assembled or reconfigured by robots moving across their surface.

Bibliography

I. Bekey. *Tethers open new space options*, volume 21. NASA, Office of Space Flight (1983), 1983.

V.V. Beletsky, E.M. Levin, and American Astronautical Society. *Dynamics of Space Tether Systems, Advances in the Astronautical Sciences*, volume 83. Univelt, August 1993.

M.P. Cartmell. Generating velocity increments by means of a spinning motorised tether. *34th AIAA/ASME/SAE/ASEE Joint Propulsion Conference and Exhibit, Dayton, Ohio, USA*, 98-3739, 13-15 July 1998.

M.P. Cartmell and S.W. Ziegler. Experimental scale model testing of a motorised momentum exchange propulsion tether. In *37th AIAA/ASME/SEA/ASEE Joint Propulsion Conference, Salt Lake City, Utah, USA, AIAA 2001-3914*, July 2001.

M.P. Cartmell, C.R. McInnes, and D.J. McKenzie. Proposals for a continuous earth-moon cargo exchange mission using the motorised momentum exchange tether concept. *Proc. XXXII International Summer School and Conference on Advanced Problems in Mechanics, APM2004*, pages 72–81, June 24 - July 1 2004.

M. L. Cosmo and E. C. Lorenzini. *Tethers in Space Handbook (3rd ed)*. Number 3. NASA Marshall Space Flight Center, Cambridge, MA, December 1997. URL `http://www.tethers.com/papers/TethersInSpace.pdf`.

Mario L. Cosmo, Enrico C. Lorenzini, and Claudio Bombardelli. Space tethers as testbeds for spacecraft formation-flying. *Advances in the Astronautical Sciences*, 119(SUPPL):1083 – 1094, 2005. ISSN 0065-3438.

C.H Draper. *Feasibility of the Motorised Momentum Exchange Tether System*. PhD thesis, University of Glasgow, June 2006.

R.L. Forward and R.P. Hoyt. Failsafe multiline hoytether lifetimes. *1st AIAA/SAE/ASME/ASEE Joint Propulsion Conference, San Diego, CA, AIAA Paper 95-28903*, July 1995.

Hironori A. Fujii, Takeo Watanabe, Tairou Kusagaya, Masanori Ohta, and Daisuke Sato. Dynamics of a crawler mass of space tether system. In *25th International Symposium on Space Technology and Science (ISTS),*

Kanazawa, Japan, 2006.

P.E. Glaser. Power from the sun, its future. *Science*, 162(3856):857–861, 1968.

N. Kaya, M. Iwashita, S. Nakasuka, L. Summerer, and J. Mankins. Crawling robots on large web in rocket experiment on furoshiki deployment. *55th International Astronautical Congress, Vancouver, Canada*, 2004a.

N. Kaya, S. Nakasuka, L. Summerer, and J. Mankins. International rocket experiment on a huge phased array antenna constructed by furoshiki satellite with robots. In *24th International Symposium on Space Technology and Science, Miyazaki, Japan*, 2004b.

Shinji Masumoto, Kuniyuki Omagari, Tomio Yamanaka, , and Saburo Matunaga. System configuration of tethered spinning solar sail for orbital experiment - numerical simulation and ground experiment. In *25th International Symposium on Space Technology and Science (ISTS), Kanazawa, Japan*, 2006.

C.R. McInnes. *Solar Sailing: Technology, Dynamics and Mission Applications*. Springer Praxis Publishing, 1999.

D.J. McKenzie and M.P. Cartmell. On the performance of a motorized tether using a ballistic launch method. *55th International Astronautical Congress, Vancouver, Canada*, (IAC-04-IAA-3.8.2.10), Oct. 4-8 2004.

A.K. Misra. Equilibrium configurations of tethered three-body systems and their stability. *The Journal of the Astronautical Sciences*, 50(3):241–253, 2002.

Y. Miyazaki and Y. Iwai. Dynamics model of solar sail membrane. In *ISAS 14th Workshop on Astrodynamics and Flight Mechanics*, 2004.

C. Murray, M.P. Cartmell, G. Radice, and M. Vasile. A mechanism for the continuous exchange of resources between the earth and the moon using a hybrid of symmetrically laden motorised momentum exchange tethers and conventional chemical propulsion systems. Technical report, Alenia-Alcatel, Departments of Mechanical & Aerospace Engineering, University of Glasgow, 2006.

T. Nakano, O. Mori, and J. Kawaguchi. Stability of spinning solar sail-craft containing a huge membrane. *AIAA Guidance, Navigation, and Control Conference and Exhibit*, pages AIAA–2005–6182, 2005.

G. B. Palmerini, S. Sgubini, and M. Sabatini. Space webs based on rotating tethered formations. In *57th International Astronautical Congress, Valencia, Spain*, 2-6th October 2006.

Gunnar Tibert and Mattias Gärdsback. Space-webs. Technical report, KTH and ESA ACT, 2006.

S.W. Ziegler. *The Rigid Body Dynamics of Tethers in Space*. PhD thesis, Department of Mechanical Engineering, University of Glasgow, 2003.

S.W. Ziegler and M.P. Cartmell. Using motorized tethers for payload orbital transfer. *Journal of Spacecraft and Rockets*, 38(6):904–913, 2001.

Appendix A

Graphics

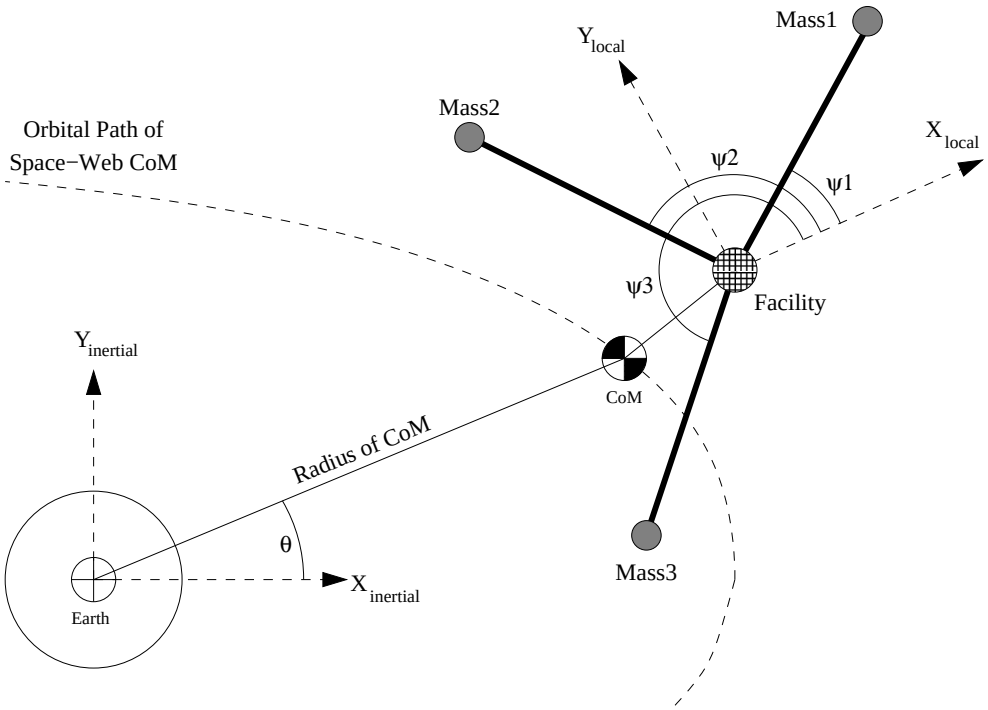

Figure A.1: Space-web diagram with 3 sub-spans shown in Inertial Space

A.1 Case 1 - CoM plots of stability while increasing web mass

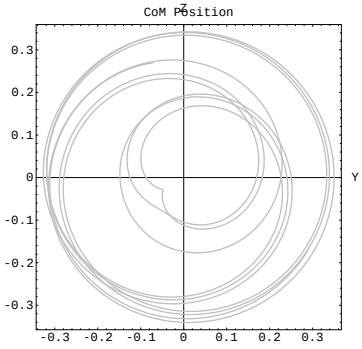

Figure A.2: $mWeb = 27kg$

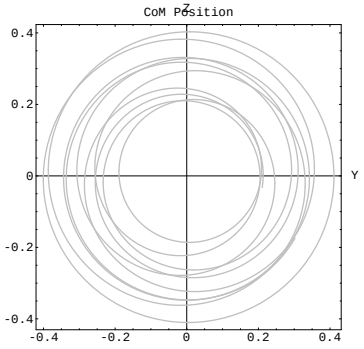

Figure A.3: $mWeb = 34kg$

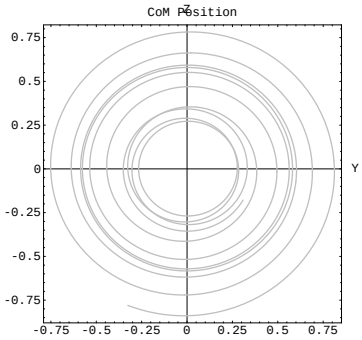

Figure A.4: $mWeb = 38kg$

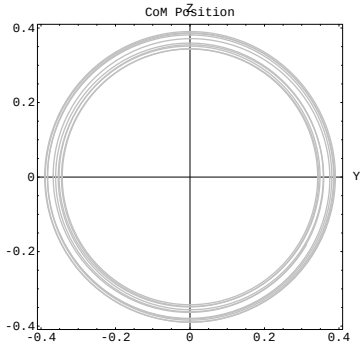

Figure A.5: $mWeb = 40kg$

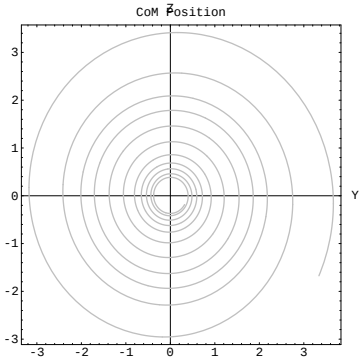

Figure A.6: $mWeb = 45kg$

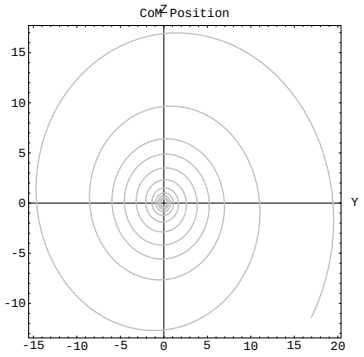

Figure A.7: $mWeb = 48kg$

A.2 Case 1 - CoM plots of stability while increasing robot mass

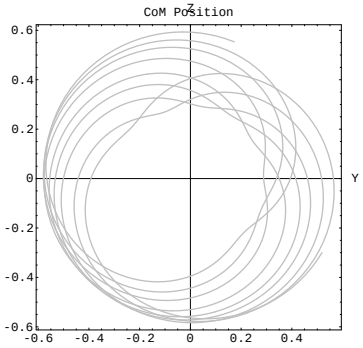

Figure A.8: $Mrobot = 10kg$

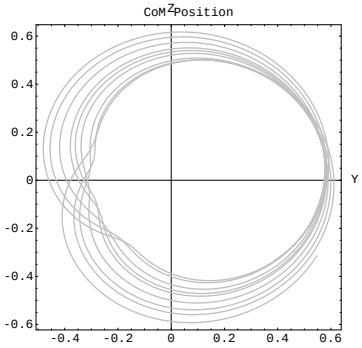

Figure A.9: $Mrobot20kg$

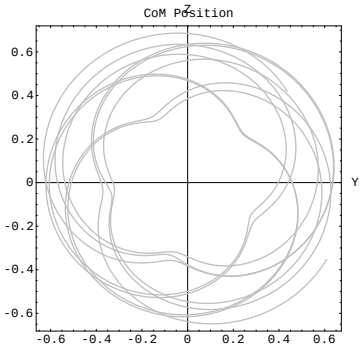

Figure A.10: $Mrobot50kg$

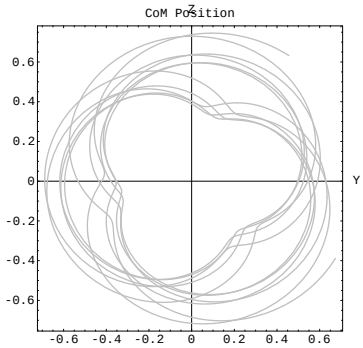

Figure A.11: $Mrobot10kg$

A.3 CoM plots of stability while changing robot paths

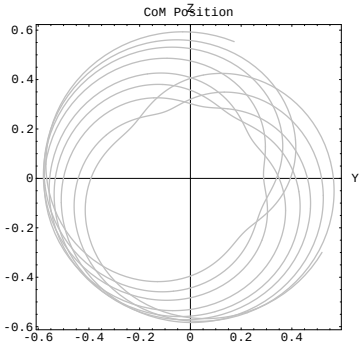

Figure A.12: Case F1

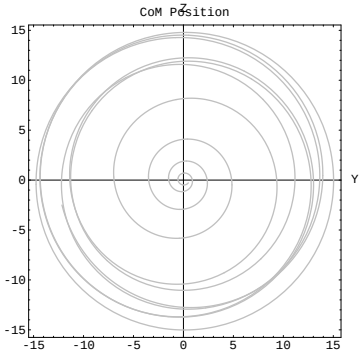

Figure A.13: Case F2

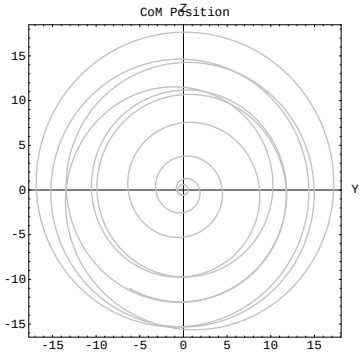

Figure A.14: Case F3

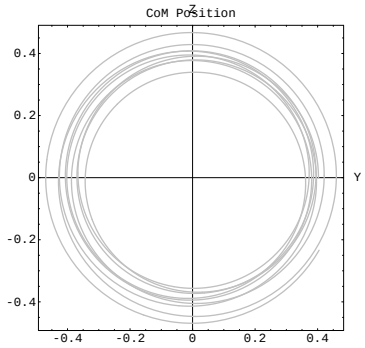

Figure A.15: Case F4

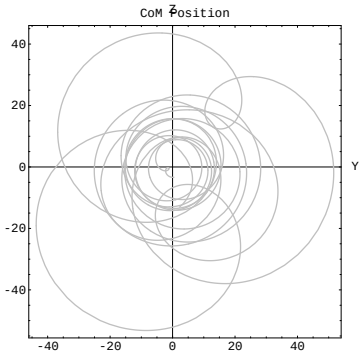

Figure A.16: Case F5

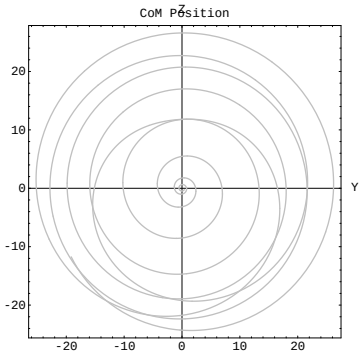

Figure A.17: Case F6

A.4 Case 6 - CoM plots of stability while decreasing robot velocity

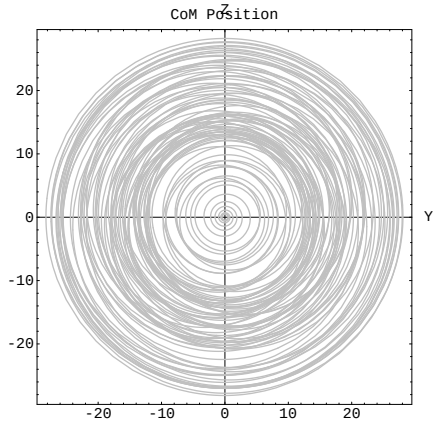

Figure A.18: $V_{robot} = 1.0\,m/s$

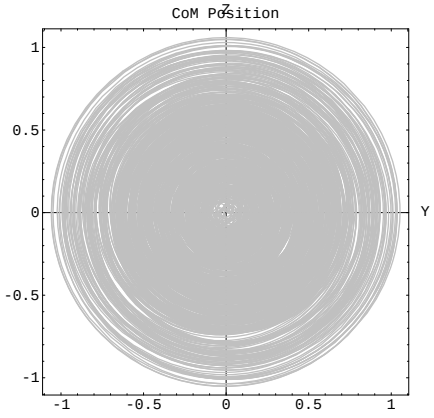

Figure A.19: $V_{robot} = 0.1\,m/s$

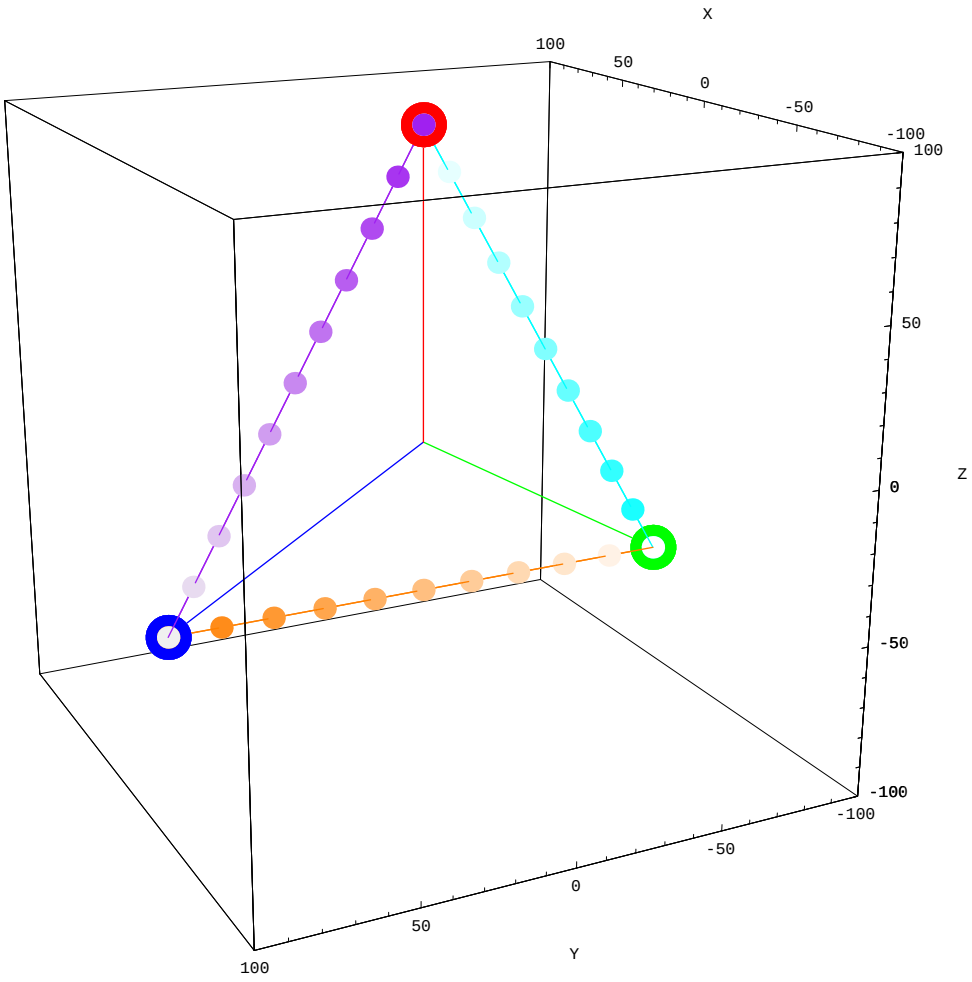

Figure A.20: Case 1 – 3 Robots moving symmetrically round the web perimeter

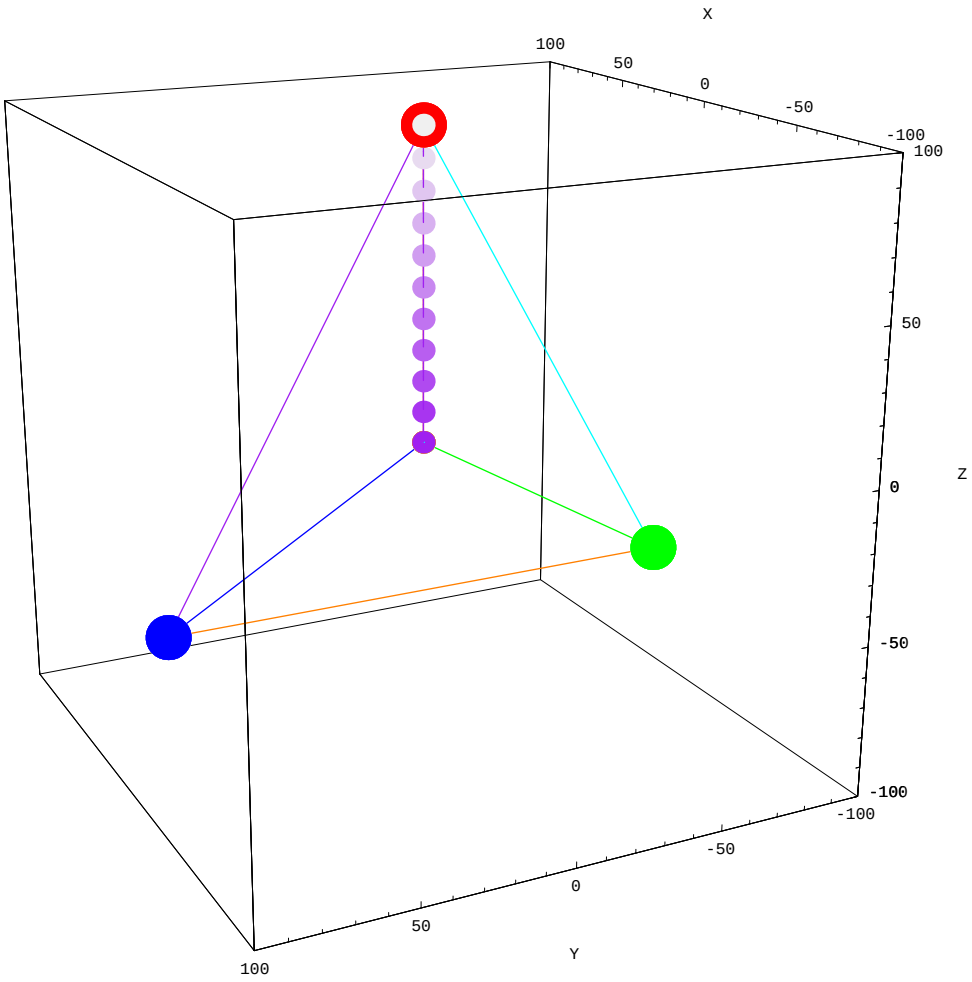

Figure A.21: Case 6 – 1 Robot moving asymmetrically along first sub-span

Appendix B

Data

Data generated during the first run phase - initially examining the dynamics of the space-web.

The units for the variables are as follows:

Mweb	Msat	MRobot	psi	dpsi/dt	k	CoM disp
kg	kg	kg	degrees	radians	N/m	m

The ICs of selected other parameters are:

$L = 100.0m$; $Mfacility = 100.0kg$; $eccent = 0.0$; $tend = 100.0s$; $R = 6.578 * 10^6 m$

run	Case	Mweb	Msat	MRobot	psi	dpsi/dt	k	CoM disp	Pred CoM	Diff%
1	1	27	10	10	0.1	0.1	1227	0.04	-0.47	-1179%
2	1	27	10	1	0.1	0.1	1227	0.03	-0.59	-1849
3	1	270	2	2	0.1	0.1	1227	45.00	48.34	107
4	1	270	10	2	0.01	1.0	1227	50.00	-287.35	-575
5	1	27	1	2	1	0.1	122.7	0.35	42.21	12059
6	1	33.75	1.25	2	1	0.1	122.7	0.42	40.20	9572
7	1	37.8	1.4	2	1	0.1	122.7	0.78	39.04	5005
8	1	40.5	1.5	2	1	0.1	122.7	0.39	38.29	9945
9	1	44.82	1.66	2	1	0.1	122.7	3.80	37.11	977
10	1	47.5	1.759259	2	1	0.1	122.7	20.00	36.40	182
11	1	54	2	2	1	0.1	122.7	34.00	34.73	102
12	1	27	1	2	1	0.1	122.7	0.51	42.21	8276
13	1	54	2	2	1	0.1	122.7	0.52	34.73	6679
14	1	135	5	2	1	0.1	122.7	0.55	21.07	3830
15	1	270	10	10	1	0.1	122.7	0.60	50.70	8450
16	1	540	20	10	1	0.1	122.7	0.63	851.23	136197
17	1	135	5	10	1	0.1	122.7	0.59	-28.33	-4802
18	1	135	10	10	1	0.1	122.7	0.59	-135.91	-23035
19	1	135	10	20	1	0.1	122.7	0.62	-298.99	-48224
20	1	135	10	50	1	0.1	122.7	0.68	-788.24	-115917
21	1	135	10	100	1	0.1	122.7	0.75	-1603.65	-213819
22	1	27	10	10	1	0.1	122.7	0.41	-285.19	-69560
23	2	27	10	10	0.1	0.1	1227	6.00	-0.47	-8
24	2	27	10	1	0.1	0.1	1227	3.00	-0.59	-20
25	2	135	10	10	1	0.1	122.7	15.00	-135.91	-906
26	3	27	10	10	0.1	0.1	1227	6.00	-0.47	-8
27	3	27	10	1	0.1	0.1	1227	3.10	-0.59	-19
28	3	135	10	10	1	0.1	122.7	17.50	-135.91	-777
29	4	27	10	10	0.1	0.1	1227	0.03	-0.47	-1572
30	4	27	10	1	0.1	0.1	1227	0.03	-0.59	-2151
31	4	135	10	10	1	0.1	122.7	0.48	-135.91	-28612
32	5	27	10	10	0.1	0.1	1227	30.00	-0.47	-2
33	5	27	10	1	0.1	0.1	1227	3.50	-0.59	-17
34	5	135	10	10	1	0.1	122.7	52.00	-135.91	-261
35	6	135	10	10	1	0.1	122.7	26.00	-135.91	-523
36	6	135	10	10	1	0.5	122.7	28.00	-913.47	-3262
37	6	2.7	10	5	1	0.5	122.7	1.10	-862.14	-78377

Data generated during the numerical investigation into stability.

run	A:Mweb	B:Msat	C:Mrobot	D:psi	E:psidot	F: CoM posn	predicted	Diff %
1	27	2	1	0.01	0.1	11.49	12.29	107%
2	270	2	1	0.01	0.1	49.41	46.71	95%
3	27	10	1	0.01	0.1	0.00	-2.70	-83118%
4	270	10	1	0.01	0.1	52.76	53.56	102%
5	27	2	10	0.01	0.1	28.09	25.39	90%
6	270	2	10	0.01	0.1	53.20	54.00	102%
7	27	10	10	0.01	0.1	0.00	0.80	19141%
8	270	10	10	0.01	0.1	55.75	53.05	95%
9	27	2	1	0.1	0.1	11.28	10.16	90%
10	270	2	1	0.1	0.1	49.83	47.37	95%
11	27	10	1	0.1	0.1	0.03	0.12	369%
12	270	10	1	0.1	0.1	52.79	51.67	98%
13	27	2	10	0.1	0.1	27.49	26.72	97%
14	270	2	10	0.1	0.1	52.99	51.65	97%
15	27	10	10	0.1	0.1	0.04	-0.05	-111%
16	270	10	10	0.1	0.1	55.61	54.83	99%
17	148.5	6	5.5	0.055	0.55	47.15	31.10	66%
18	148.5	6	5.5	0.055	0.55	47.15	31.10	66%
19	148.5	6	5.5	0.055	0.55	47.15	31.10	66%
20	148.5	6	5.5	0.055	0.55	47.15	31.10	66%
21	27	2	1	0.01	1	49.41	46.71	95%
22	270	2	1	0.01	1	49.86	50.66	102%
23	27	10	1	0.01	1	0.00	0.80	24649%
24	270	10	1	0.01	1	0.00	-2.70	-64127%
25	27	2	10	0.01	1	33.10	33.90	102%
26	270	2	10	0.01	1	49.41	46.71	95%
27	27	10	10	0.01	1	49.83	47.13	95%
28	270	10	10	0.01	1	55.77	56.57	101%
29	27	2	1	0.1	1	49.41	48.63	98%
30	270	2	1	0.1	1	49.82	48.69	98%
31	27	10	1	0.1	1	0.03	-1.09	-3346%
32	270	10	1	0.1	1	0.03	-0.74	-2287%
33	27	2	10	0.1	1	33.11	31.98	97%
34	270	2	10	0.1	1	49.41	48.63	98%
35	27	10	10	0.1	1	0.00	-0.77	-18329%
36	270	10	10	0.1	1	55.76	54.63	98%

The ICs of selected other parameters are:

$L = 100.0m$; $Mfacility = 100.0kg$; $eccent = 0.0$; $tend = 100.0s$; $R = 6.578 * 10^6 m$

Note: the percentage change (= predicted CoM / simulated CoM) may be very large due to the small simulated CoM displacement.

Data generated during the numerical investigation into stability.

Term	Effect	Stdized Effect	SumSqr	% Contribtn
A-Mweb	-	27.21	7182.9	37.72
B-Msat	+	-16.57	2447.8	12.85
AE	+	-15.32	1869.6	9.82
BCE	-	14.34	1656.8	8.70
C-Mrobot	-	10.90	872.3	4.58
BC	-	9.93	666.4	3.50
BE	+	-8.69	686.3	3.60
AB	-	7.21	435.0	2.28
ACE	-	6.98	346.3	1.82
CE	-	5.04	232.9	1.22
AC	-	4.66	193.2	1.01
ABE	+	-3.76	118.3	0.62
ABC	-	3.75	118.6	0.62
BDE	+	-3.37	93.4	0.49
ADE	-	3.29	117.6	0.62
ABCDE	-	3.19	85.1	0.45
ACD	-	3.17	99.5	0.52
BCD	+	-3.15	102.7	0.54
CDE	+	-3.12	92.4	0.49
ABDE	-	3.12	81.5	0.43
CD	+	-3.09	110.1	0.58
D-psi	+	-3.08	79.6	0.42
BCDE	+	-3.08	83.7	0.44
ACDE	-	3.04	89.0	0.47
ABCD	-	3.02	61.5	0.32
DE	+	-3.00	75.6	0.40
ABD	-	2.97	74.0	0.39
AD	-	2.93	98.7	0.52
BD	+	-2.84	34.2	0.18
E-psidot	-	1.48	18.3	0.10
Lack Of Fit			9.6	0.05
Pure Error			0.0	0.00

The 'Effect' term in column 2 is a reflection on the stabilising (+) or destabilising (−) effect of the term.